Journal of Optoelectronics and Advanced Materials Vol. 7, No. 1, February 2005, p. 231 – 236

Invited Paper

HIGH-CURRENT PULSED ARC PREPARATION OF CARBON AND METAL-CARBON NANOPARTICLES

S. Muhl*, F. Maya, S. Rodil, G. Gonzalez E. Camps[a], L. Escobar-Alarcon[a], M. Espinosa-Pesqueira[a]

Instituto de Investigaciones en Materiales, UNAM, D.F. 04510, México, México
[a]Instituto Nacional de Investigaciones Nucleares, Edo. de México, México, México

We report the preparation of graphite and carbon-metal clusters by high-current pulsed arc evaporation of the electrodes used. Experiments were performed as a function of the gas pressure and type, for the graphite electrodes, and the metal type used as one of the electrodes, for the carbon-metal particles. The maximum arc current was varied by controlling the circuit resistance and the charge voltage of the bank of capacitors (total capacitance 0.5 F). The deposits were studied by AFM, SEM and TEM, and the chemical analysis of the deposits was performed using XPS and EDX. Most experiments were carried out at atmospheric pressure, but both the effect of the ambient pressure and gas type, air, helium and argon were studied for conditions that had been found to be efficient for the cluster production.

(Received December 9, 2004; accepted January 26, 2005)

Keywords: Pulsed Arc, Carbon nanoparticles, Encapsulated metal nanoparticles

1. Introduction

The discovery of the formation of diverse nanostructured forms of carbon by the Kratschmer-Huffman carbon arc method [1] and the modifications developed by Dravid *et al.* [2,3] have together generated a strong interest in the production of nanostructured materials for many applications [4,5]. The techniques have been used to produce not only carbonaceous materials but also a wide range of encapsulated metal nanoparticles (EMN´s) [6,7,8,9]. Most of this work has been performed using DC continuous arcs, with currents of around 100A in a He, Ar or hydrogen atmosphere at 200-500 Torr [10,11]. However, there are a few reports of the advantages of using pulsed arcs in the same current range [12,13,14]. Even with the great interest, the formation process of the clusters and nanoparticles is not clearly understood [14]. In this paper, we report the formation of carbon nanoparticles and EMN´s using a high-current pulsed arc system; ≥ 1000 A. Under these conditions, not only is there sufficient energy to evaporate the electrode materials but also much higher energy plasmas are created.

2. Experimental details

The experimental apparatus is described in detail elsewhere [15]. For the experiments on carbon deposits, two 0.6 mm diameter graphite rods were machined from 3.12 mm diameter high purity AERO graphite from ESPI; the thin part of the rods was typically 5 mm long. For the metal carbon work, 3.12 mm diameter carbon electrodes with various diameters and types of metal wire were used. The maximum arc current and its temporal form were sensed by measuring the voltage drop across a low inductance 0.98 mΩ resistor in the arc circuit, connected to a HP54522A Digital

* Corresponding author: muhl@servidor.unam.mx

oscilloscope. An analysis of the I/V curves showed that the circuit inductance and the arc power at a charge voltage of 80 V was typically 163 kW.

For the carbon experiments, two silicon or highly polished stainless steel substrates were used, one placed 8 mm from the arc and the other 6 cm from the arc on a water-cooled copper block which was connected to a DC power supply to bias the substrate relative to the graphite. Deposits were produced in air from 45 mTorr to atmospheric pressure and in helium and argon at 100, 300 and 500 Torr. For the metal-carbon study, the arc was created in air at atmospheric pressure within a 20 mm diameter piece of glass tubing. For the TEM analysis, the deposit was removed from the inside of the tube by agitation in methanol using an ultrasonic bath. Drops of this liquid were then applied to a TEM grid coated with a holey polymer layer. For the SEM work, a +500 V biased substrate of polished stainless steel was used. Experiments were performed using 1 cm long pieces of 1 mm diameter wire of Ti, W, Cu, Ag and 316 stainless steel.

The deposits were characterised by X-ray diffraction using a Siemens D500 difractometer, TEM, SEM, EDX, AFM Auto Probe CP system of Park Scientific Instruments. Additionally, XPS analysis was carried out using a Thermo VG MultiLab ESCA 2000 system with a CLAM4 MCD analyzer and a MgK_α ($h\nu$ = 1253.6 eV) X-ray source. The peak FWFM was 1.2 eV, and the spectra were calibrated relative to the surface oxygen peak.

3. Results and discussion

31.1 Carbon deposits

Our earlier work using shadowgraphy and optical emission spectroscopy indicated that (i) bi-atomic carbon molecules and electrons were the principal particles emitted by the arc evaporation, (ii) the effective refractive index of the volume around the arc could be modelled as containing carbon particles of approximately 250 nm diameter at atmospheric pressure, and (iii) the particle size decreased with decreasing gas pressure [15]. To confirm the results of the simulation, samples were deposited on polish stainless steel as a function of pressure in air, He and Ar. SEM micrograph images of the deposits prepared at a selection of gas pressures are shown in Fig. 1. The digitised images of the deposits were analysed, and the average particle diameter as a function of the gas pressure is presented in Fig. 2. The diameter of the particles prepared at atmospheric pressure in air can be seen to be about 120 nm. Considering the assumptions used in the analysis of the shadowgraph, based on Mie scattering, this is in reasonable agreement with

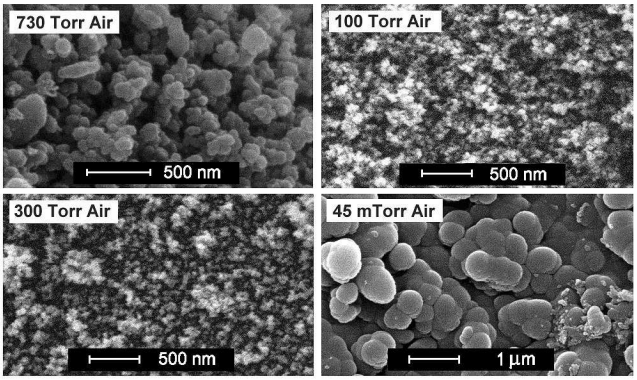

Fig. 1. SEM micrographs of particles of carbon produced in air at the pressures shown, using a ~1200 A - 40 ms arc between two 0.6 mm diameter graphite electrodes.

the simulated value. The particle diameter was found to decrease almost linearly with the logarithm of the gas pressure, except for the lowest pressure of 45 mTorr where the diameter was ~ 487 nm and the particles were notably more spherical. Fig. 3 shows a TEM image and electron diffraction pattern of the particles deposited using a ~ 1200 A arc in air. The pattern can be indexed to that of graphite, and the bright diffraction lines in the image (these were seen to translate across the particles as the sample was tilted) indicate that the particles are monocrystals of graphite. Fig. 4 shows an AFM image of part of one of these particles, the distance between adjacent minima or maxima in the image is 1.33 nm, which is twice the c-axis of the hexagonal unit cell of graphite.

Deposits were carried out in air using 5 arcs of ~1200 Å, as a function of the substrate bias from –600 to +600V The weight of the stainless steel substrate was measured before and after the deposition.

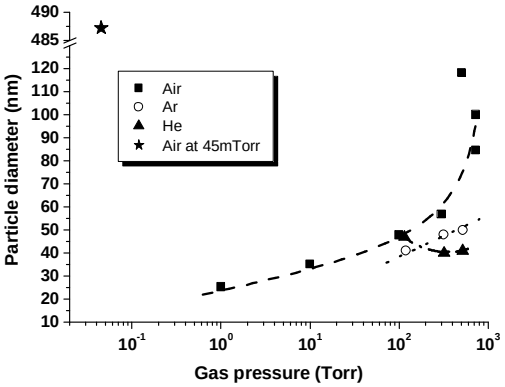

Fig. 2. The carbon particle diameter versus gas pressure for particles produced using a ~ 1200 A -40 ms arc between two 0.6 mm diameter graphite electrodes, in air, helium and argon.

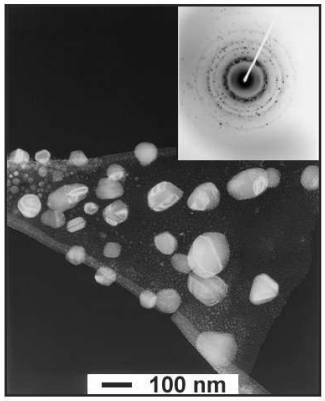

Fig. 3. TEM bright field image of the carbon particles, together with their electron diffraction pattern.

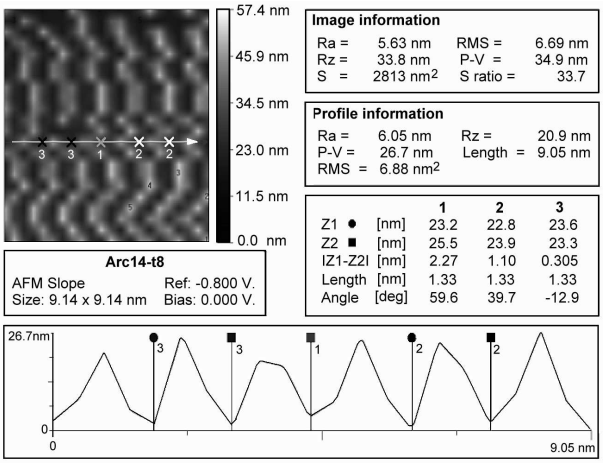

Fig. 4. The AFM image and analysis of the carbon particles.

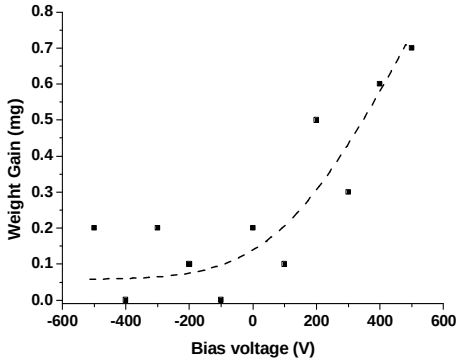

Fig. 5. The substrate weight gain per arc as a function of the substrate bias used in the deposition of the carbon particles.

Fig. 5 shows the results of this study. The weight gain per arc for a negative bias is approximately constant. However, a significant increase was observed for positive values, indicating that the carbon particles had a negative charge. The results lead us to consider that (i) the bi-atomic carbon molecules emitted from the surfaces of the graphite rods by the arc suffer collisions with the surrounding gas molecules, causing the formation of larger carbon molecules, (ii) this process continues during the ~ 40 ms lifetime of the arc and furthermore, (iii) as these larger molecules travel outwards, a sequence of collisions and coalescences of particles occurs until the 120 nm clusters are created and deposited. At lower pressures, the mean free path of the molecules/particles increases, leading to fewer collisions and the accumulation of less material and therefore the deposition of smaller clusters. Within the arc plasma, the electron density is very high and the relatively large clusters can easily capture electrons and accumulate a net negative charge. This phenomenon is an example of a dusty plasma, as discussed recently ([16] and references therein). However, at a pressure of 45 mTorr, the mean free path is approximately equal to the rod-to-substrate distance. Therefore, the bi-atomic molecules arrive at the substrate with few collisions with the gas molecules. The high-energy environment at the substrate surface (electron and photon fluxes) is probably responsible for the formation of the spherical smooth carbon particles. Further experiments are planned in the near future to study this formation process.

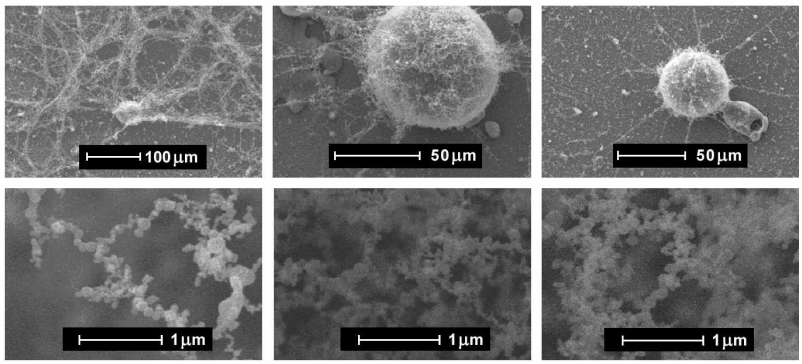

Fig. 6. SEM micrographs of the material deposited by a ~ 1000 A - 40 ms arc between a graphite electrode and copper, stainless steel or tungsten wires.

3.2. Metal-carbon deposits

Fig. 6 shows low and high magnification SEM images of deposits formed using Cu, W and stainless steel electrodes. Independently of the metal used, the deposits formed strings of metal-carbon spheres, which at low magnification appear as long fibres. The composition of the fibres obtained by EDX is given in Table 1 for the Cu and W cases. It is interesting to note that the carbon content of the Cu spheres is higher than that of the W ones, even though Cu does not form a stable carbide.

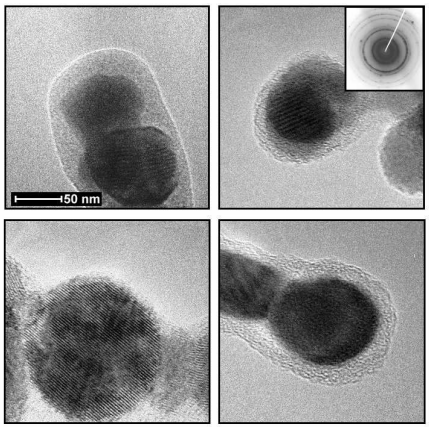

Fig. 7. TEM images of the encapsulated metal particles.

Fig. 7 shows a selection of TEM images of the particles deposited using W and Ag. Again, independently of the electrode type, it can be seen that in each case the particles consist of a crystalline metal-containing nucleus of approximately 80 nm, coated with amorphous carbon. The d-spacings obtained from the electron diffraction pattern of the Ag-C particles do not agree with those of Ag, graphite or diamond, but appear to be from a mixture of various silver oxides.

Table 1 shows the results of the XPS and EDX compositional analyses of the metal-C particles. Fig. 8 shows part of the spectra obtained from the XPS analysis of the W-C, Ag-C and Ti-C clusters. It is clear that the metal nucleus is a mixture of pure metal and oxide, in agreement with the diffraction results, with almost no formation of the metal carbide, and that the carbon content of the particles is approximately 70 at.% in each case.

There is a considerable difference between the composition values from EDX and XPS, but this is due to the experimental differences in the measurements. The EDX analysis was performed on particles deposited on metal substrates, and therefore includes information from any undercoat below the particles. The XPS analysis was of particles that had been separated from the substrate.

Table 1. The compositional analysis of the encapsulated metal nanoparticles.

Ti-C Particles			W-C Particles			Ag-C Particles			Cu-C Particles		
	Atomic%			Atomic%			Atomic%			Atomic%	
	EDX	XPS		EDX	XPS		EDX	XPS		EDX	XPS
Ti	24	3.1	W	8	9.1	Ag	41	4.1	Cu	46	-
O	35	19.6	O	14	14.2	O	4	27.3	O	10	-
C	41	77.4	C	78	76.7	C	55	68.5	C	44	-

4. Conclusions

The high current pulsed arc evaporation of carbon from thin graphite electrodes in air initiates with the emission of carbon bi-atomic molecules. These collide with the gas molecules, causing agglomeration of the molecules until ~120 nm monocrystalline graphite clusters are formed. The type of gas and the pressure control the collision process and, therefore the cluster sizes depend strongly on these parameters. If the gas pressure is such that the mean free path between collisions is at least equal to the electrode-substrate separation, the cluster formation is controlled by the high energy density at the substrate surface.

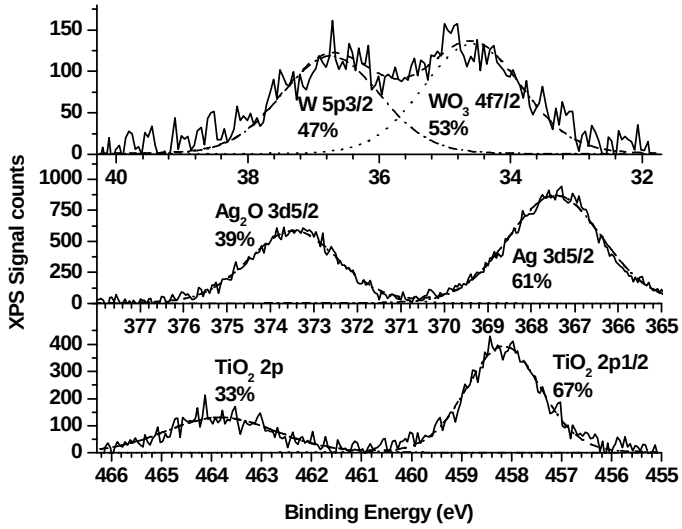

Fig. 8. The XPS spectra of the silver, titanium and tungsten encapsulated metal particles, showing the proportion of the different phases present.

Encapsulated metal nanoparticles can be formed by the joint evaporation of carbon and metal electrodes. The formation process in this case appears to be the simultaneous reaction of the metal with oxygen and the gas phase condensation of the metal+oxide. These small particles are then covered by amorphous carbon, as an outer shell. In this case, the metal nucleus is crystalline, but more work is needed to satisfactorily identify the crystalline phase present. The deposited EMNs self-align as fibres during the deposition process, independently of the metal used. However, as yet no clear understanding of this phenomenon is available. Due to the size of the particle and the high density of electrons in the arc plasma, the clusters accumulate a negative charge, which facilitates the deposit collection.

References

[1] W. Kratschmer, L. D. Lamb, K. Fostiropoulos, D.R. Huffman, Nature **347,** 354 (1990).
[2] V. P. Dravid, J. J. Host, M. Teng, B. Elliot, J. Hwang, D. L. Johnson, T. O. Mason, J. R. Weertman, Nature **374,** 602 (1995).
[3] J. J. Host, M. J. Teng, B. Elliot, J. Hwang, T. O. Mason, D. L. Johnson, V. P. Dravid, J. Mater. Res. **12,** 1268 (1997).
[4] T. Hayashi, S. Hironi, M. Tomita, S. Umemura, Nature **381,** 772 (1996).
[5] H. Wang, S. P. Wong, in: H. S. Nalwa (Ed.), Magnetic Nanostructures, American Scientific Publishers, Stevenson Ranch, CA, 2002 and references therein (Chapter 10).
[6] J. M. Bonard, S. Seraphin, J. E. Wegromwe, J. Jiao, A. Chatelain, Chem. Phys. Lett. **343,** 251 (2001).
[7] M. Jiang, X. Gao Zhang, Y. Liu, G. Ming Hao, J. Lin, Mats. Sci. & Eng. **B87,** 66 (2001).
[8] J. Ling, Y. Liu, G. Hao, X. Zhang, Mats. Sci. & Eng. **B100,** 186 (2003).
[9] Y. Saito, T. Matsumoto, K. Nishikubo, J. Cryst. Growth **172**, 163 (1997).
[10] Z. Cui, Z. Zhang, C. Hao, L. Dong, Z. Meng, L. Yu, Thin Solid Films **318,** 76 (1998).
[11] Y. Saito, T. Matsumoto, K. Nishikubo, Carbon **35,** 1757 (1997).
[12] H. Wang, M.F. Chiah, W.Y. Cheung, S.P. Wong, Physica **B344,** 88 (2004).
[13] T. Yamaguchi, S. Bandow, S. Iijima, Chem. Phys. Lett. **389,** 181 (2004).
[14] Y. Murooka, Y. Maede, M. Ozaki, M. Hibino, Chem. Phys. Lett. **341,** 455 (2001).
[15] S. Muhl, F. Maya, S. E. Rodil, E. Camps, M. Villagran, A. Garcia. Thin Solid Films **433**, 50 (2003).
[16] R. L. Merlino, J. A. Goree, Physics Today, **July**, 32 (2004). Publishers American Institute of Physics, New York, NY, USA.

.